
Open-Canopy: A Country-Scale Benchmark for Canopy Height Estimation at Very High Resolution

Fajwel Fogel⁴Yohann Perron^{3,5}Nikola Besic²Laurent Saint-André⁷Agnès Pellissier-Tanon¹Martin Schwartz¹Thomas Boudras¹Ibrahim Fayad^{1,6}Alexandre d'Aspremont^{4,6}¹ LSCE/IPSL, CEA-CNRS-UVSQ² LIF, IGN, ENSGLoic Landrieu³³ LIGM, Ecole des Ponts, CNRS, UGE⁴ CNRS & École Normale Supérieure⁷ INRAE, BEFPhillipe Ciais¹⁵ EFEO⁶ Kayyros

Abstract

Estimating canopy height and canopy height change at meter resolution from satellite imagery has numerous applications, such as monitoring forest health, logging activities, wood resources, and carbon stocks. However, many existing forest datasets are based on commercial or closed data sources, restricting the reproducibility and evaluation of new approaches. To address this gap, we introduce Open-Canopy, the first open-access and country-scale benchmark for very high resolution (1.5 m) canopy height estimation. Covering more than 87,000 km² across France, Open-Canopy combines SPOT satellite imagery with high resolution aerial LiDAR data. We also propose Open-Canopy- Δ , the first benchmark for canopy height change detection between two images taken at different years, a particularly challenging task even for recent models. To establish a robust foundation for these benchmarks, we evaluate a comprehensive list of state-of-the-art computer vision models for canopy height estimation. The dataset and associated codes can be accessed at <https://github.com/fajwel/Open-Canopy>.

1 Introduction

National and regional forestry agencies have traditionally developed their management strategies around a 10 to 20-year planning cycle [1, 2]. However, the accelerating pace of climate change requires a shift towards more responsive forest management practices [3, 4, 5]. This implies monitoring the evolution of forest resources at a national level with high spatial resolution and, ideally, on a yearly basis. Although Aerial Laser Scanning (ALS) provides rich information about canopy height [6], its high cost and logistic requirements make annual campaigns unrealistic. However, the acquired ALS data can be used to train machine learning models to estimate canopy height from a single Very High Resolution (VHR) satellite image, offering a cost-effective alternative for annual monitoring. To support the evaluation and development of these tools, we introduce Open-Canopy, an open-access dataset specifically designed for VHR canopy height estimation. In addition, we propose the first benchmark for the task of estimating the canopy height change between two images.

High-Resolution Canopy Height Estimation. The spatial and temporal resolution of canopy height estimation is critical to several of its key applications. As seen in Figure 1, higher spatial resolution enables the detection of smaller vegetation, such as shrubs and hedges [13], which play a vital role in ecosystem health [14]. Furthermore, observations at scales close to individual trees lead to insights into biodiversity [15] and a more accurate proxy for biomass estimation [16].

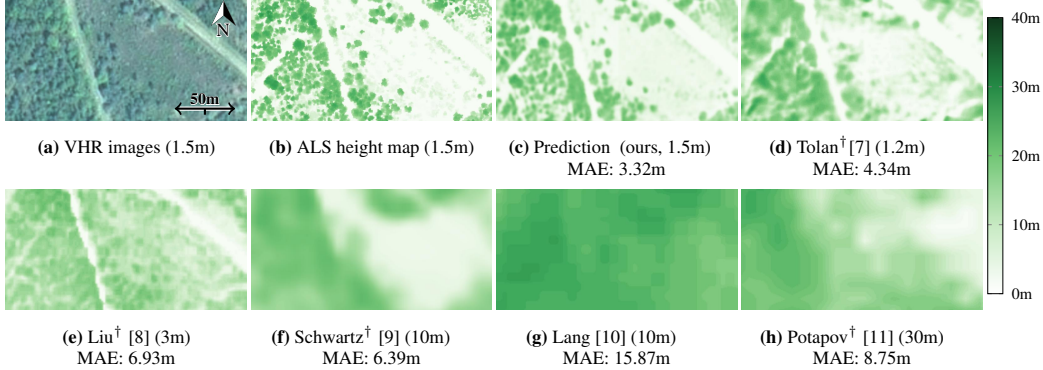


Figure 1: Canopy Height Estimation. We represent a VHR image from the Open-Canopy test set (a), alongside its corresponding ALS-derived canopy height (b). We also include the height map predicted by a PVPTv2 [12] model trained on the Open-Canopy train set (c), compared against other canopy height products (d-h). We provide the spatial resolution and the Mean Absolute Error (MAE) for the pixels within the image’s vegetation mask (see Section 3.1). † indicates that the data or the model used to generate this maps is not open-access.

The benefit of estimating canopy height at repeated intervals from multiple satellite images allows for monitoring forest growth or decline over time. Tracking these changes is crucial for understanding forest health dynamics [17, 18], detecting tree mortality due to disturbances [19], and removals from both harvest [20] and illegal logging activities [21, 22]. In addition, it supports the creation of maps of biomass carbon stock essential for national inventories [23, 24, 25]. High-resolution growth monitoring enables the detection of specific forest management practices beyond the more visible disturbances, such as clear-cutting. Selective logging, for example, can be identified [26, 27], thereby improving forest management and conservation efforts.

The Open-Canopy Benchmark. Recent advancements in deep learning have enabled the prediction of canopy heights from satellite images. The spaceborne LiDAR GEDI [28] has been particularly transformative, allowing models to generate global canopy height maps [29], although typically at lower resolutions of 10 to 30m per pixel [9, 10, 11]. Additionally, high-resolution height maps derived from ALS data, when paired with VHR imagery, can be used to train canopy height prediction models [7, 8, 30]. However, with the notable exception of Lang et al. [10], these research efforts do not make their datasets readily accessible. The locations of training and testing sets are often undisclosed, substantial pre-processing of the data is required, and in some cases, the data depend on costly commercial imagery. Leveraging recent open-source initiatives by the French government [31, 32], we propose Open-Canopy, an open-access and country-scale canopy height benchmark with VHR satellite imagery (1.5m resolution) and ALS-based supervision, covering 87,400 km² in France. We provide ready-to-use data, official train and test splits, and all pre-processing scripts.

We also propose Open-Canopy- Δ , the first benchmark for forest height change detection. The task consists in detecting areas with significant reduction in canopy height between two consecutive VHR satellite images taken in 2022 and 2023. The ground truth was derived from two ALS acquisitions and covers a 166km² area of France.

Canopy Height Estimation Models. While the majority of existing studies in canopy height estimation have focused on UNet-type architectures [33], we propose to evaluate various modern architectures for dense predictions, including Vision Transformers (ViT)-based architectures [34] and several vision foundation models.

Our contributions are as follows:

- **Open-Canopy.** We propose a novel open-access benchmark for canopy height estimation from VHR images with dense ALS annotations.
- **Extensive Evaluations.** We evaluate several recent computer vision architectures.
- **Open-Canopy- Δ .** We propose the first benchmark for detecting significant canopy height changes between two images.

Table 1: Existing Forestry Datasets. We detail existing datasets used to train and evaluate canopy height estimation models. We report information about the satellite images used as input, the canopy height maps used to train and evaluate models, and the number of ground truth elevation data points (samples). We denote open-access and directly downloadable data sources with \checkmark , while data under commercial license are denoted with $\$$. Data sources that necessitate special access are denoted with 🔒 , complex preprocessing with ✖ , and for which the location of the train/test sets are missing with ∅ . S1/S2 refer to Sentinel 1 [35] and 2 [36] and NAIP to the National Agriculture Imagery Program [37].

Dataset	code		extent		observations			annotations		
	OA	scope	surface $\times 10^3 \text{ km}^2$	nature	res. in m	OA	nature	res. in m	samples $\times 10^6 \text{ pts}$	OA
Schwartz [9]	✗	France	588	S1/S2	10	∅	GEDI	25	90	$\text{✖} \text{∅}$
Lang [10]	\checkmark	Global	13,500	S2	10	\checkmark	GEDI	25	600	\checkmark
Potapov [11]	✗	Global	150,000	Landsat	30	∅	GEDI	25	372	$\text{✖} \text{∅}$
Tolan [7]	✗	US	5.8	MAXAR	1.2	$\text{\$}$	ALS	1	5800	\checkmark
Wagner [30]	✗	US	3.8	NAIP	0.6	$\text{🔒} \text{∅}$	ALS	1	3784	∅
Liu [8]	✗	Europe	700	Planet	3	$\text{🔒} \text{∅}$	ALS	3	77,777	∅
Open-Canopy \checkmark	\checkmark	France	87	SPOT 6-7	1.5	\checkmark	ALS	1.5	38,876	\checkmark

2 Related Work

This section details existing datasets and methods for the problem of canopy height estimation, grouped by annotation type: GEDI or ALS. See Table 1 for an exhaustive comparison of Open-Canopy with these datasets.

GEDI-Based Datasets. The Global Ecosystem Dynamics Investigation (GEDI) mission consists of a LiDAR mounted on the ISS and provides global canopy height measurements with a footprint diameter of 25m [28]. GEDI captures a set of spatially discrete full waveform echoes along paths approximately 4 km wide, offering sparse yet rich information about the vegetation structure. Models trained with GEDI data use it as a sparse and coarse supervisory signal to predict canopy heights from medium to high resolution imagery such as Landsat images at 30m resolution (Potapov [11]) or Sentinel-2 at 10 m resolution (Schwartz [9] and Lang [10]). However, GEDI’s full waveform LiDAR has registration errors of typically 10m [38].

ALS-Based Datasets. Aerial Laser Scanning (ALS) uses low-flying aircraft equipped with LiDAR to create dense 3D point clouds of the Earth’s surface. These systems typically capture data at resolutions ranging from 10 to 60 points per square meter. This data is then rasterized along a high resolution grid, and used to estimate canopy height by subtracting the lowest quantile height (ground surface) from the height of the highest quantile (top of canopy). This allows the computation of “true” height maps at scales such as 1.2m for Tolan [7] and Wagner [30], 3 m for Liu [8]. Open-Canopy use ALS data from the LiDAR-HD [31] program rasterized at 1.5 m. These maps are then used as ground truth to train models that predict canopy height from corresponding VHR images.

Canopy Height Estimation Models. Most canopy height prediction models employ fully supervised UNets [33] for their ease of use. The recent work by Tolan *et al.* uses a Vision Transformer (ViT) [34] pretrained in a self-supervised fashion [39] on 18 million images without ALS height data. In this paper, we benchmark a variety of modern deep learning architectures for dense prediction of VHR canopy height from SPOT images, including Unet [33], Vision Transformers (ViT) [34], and their hierarchical variants [12, 40, 41]. We also explore how their pretraining impact their ability to adapt from vision-related problems to the completely different task of canopy height estimation.

Canopy Height Change Estimation. As forests experience rapid losses [42, 43], better understanding and monitoring of forest dynamics is critical [44]. While existing studies have explored the long-term evolution of forests [45, 46, 47], they focus on environmental or phenological variables and low resolution (500m) imagery [48]. Forest change detection models generally operate at medium or high resolutions (10-30m) [49, 50]. Few attempts have been made to measure forest volume [51] or volume changes [52], using UAVs over small areas and without providing open-access data or code. In contrast, we introduce the first open-access, large-scale VHR benchmark for canopy height change detection with LiDAR-derived ground truth.

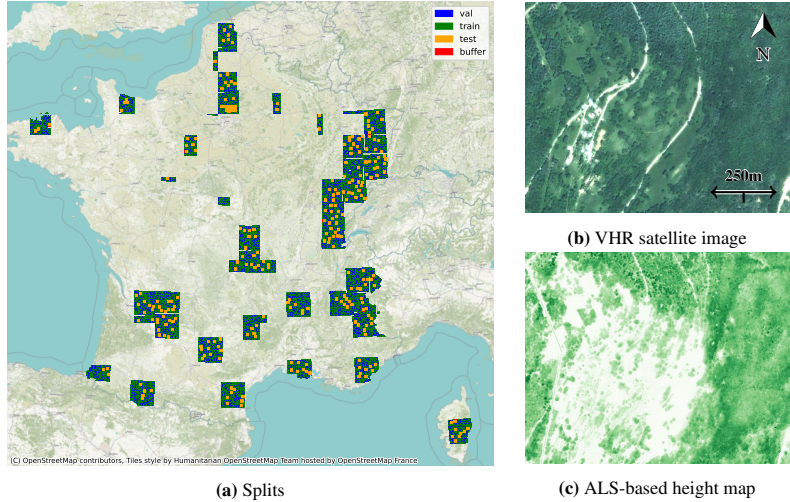


Figure 2: Open-Canopy. Our training, validation, and test sets cover most of the French territory and use a 1km buffer (a). For each tile, we provide VHR images at a 1.5 m resolution (b) and associated LiDAR-derived canopy height maps (c) .

Data Access Policies. The six studies in Table 1 all provide open-access predicted canopy height maps and often their trained models. However, only the work of Lang *et al.* provides its code and direct download links for their processed datasets. In contrast, the datasets used by Tolan *et al.*, Wagner *et al.*, and Liu *et al.* involve commercial satellite imagery or data that requires special access and cannot be redistributed. Although GEDI, Sentinel, and Landsat data are open-access, their preprocessing necessitates substantial expertise. Except for the studies of Tolan *et al.* and Lang *et al.*, these works also do not specify their training and testing splits, complicating their evaluation on external datasets due to potential overlap. Like the study of Lang *et al.*, our data, code, splits, and models are freely available. This transparency is crucial for advancing canopy height estimation as a mainstream application of vision models.

3 The Open-Canopy Benchmark: Estimating Canopy Height

We introduce Open-Canopy, an open-access country-scale benchmark for estimating canopy height at very high resolution. We first present our dataset (Section 3.1), then the models evaluated (Section 3.2). Finally, we present the results (Section 3.2) and limitations (Section 3.4) of the benchmark.

3.1 Dataset Characteristics

We present here the main characteristics of the dataset of the Open-Canopy benchmark. We report a detailed description of the dataset construction in the supplementary.

Why Just France? France offers a valuable test bed for canopy height estimation thanks to recent national open-source initiatives providing access to two critical data sources under the open EtaLab2.0 licence [53]: (i) DINAMIS [32], which supplies SPOT 6-7 VHR satellite imagery covering all of French territory at a 1.5 m resolution, and (ii) the LiDAR-HD project [31], offering airborne 3D point clouds with a density above 10 points per square meter. This combination of open-access VHR and ALS allows us to build not only a very high resolution canopy height map with a method that can be applied to the whole country, but it also makes it possible to produce maps of height changes, giving insights on recent tree removals from harvest and natural mortality.

The French metropolitan territory exhibits a wide range of climates—12 of the 18 Köppen-Geiger climate types found in continental Europe [54], including temperate, Mediterranean, and alpine environments. The French forest inventory lists 190 distinct tree species [55]. While models trained on the Open-Canopy dataset may not generalize globally, their performance within central Europe is likely to be robust given this environmental diversity.

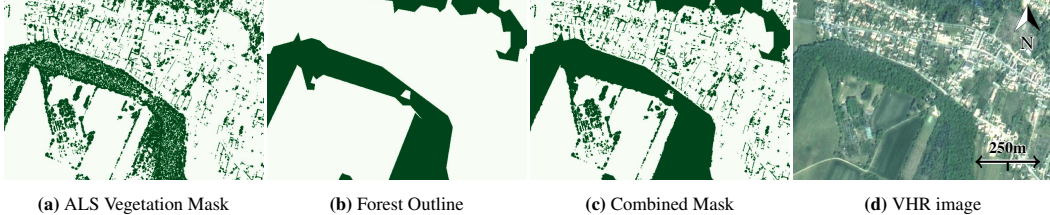


Figure 3: Vegetation Mask. We combine an ALS-derived vegetation mask (a) with official forest outlines (b) to build a pixel-precise mask (c) covering a wide range of vegetation types, as seen in the VHR image (d).

Extent and Splits. We selected 87,383 tiles, each measuring $1 \times 1 \text{ km}^2$, and spanning a total area of $87,383 \text{ km}^2$ across France. We divided the dataset into training ($66,339 \text{ km}^2$), validation ($7,369 \text{ km}^2$), and test sets ($13,675 \text{ km}^2$). We added a 1 km buffer between the test split and other splits to avoid data contamination ($8,046 \text{ km}^2$). Test tiles consist in squares of $7 \times 7 \text{ km}^2$ spread across all bioclimatic regions of France [56], with the exception of the larger test area of Chantilly forest, which we use for both height and change evaluation.

VHR Satellite Images. As illustrated in Figure 2b, we use orthorectified SPOT 6-7 images [57, 58] from Dinamis [32] with four spectral bands: red, green, blue, and near-infrared at a resolution of 6m, and a panspectral band at a resolution of 1.5m. We apply pansharpening with the weighted Brovey algorithm [59] to upsample all four spectral bands to a resolution of 1.5m. We select images from the same year as the corresponding ALS acquisition campaign, in 2021, 2022 and 2023.

ALS-Based Canopy Height. As depicted in Figure 2c, we use open-access ALS data from the LiDAR-HD acquisition campaigns [31] between 2021 and 2023, which provides a minimum density of 10 points per m^2 . The canopy height maps are calculated at the same resolution as the VHR images by taking the maximum difference between the height of each point height and the one of the nearest point classified as ground within its pixel, interpolating values in areas without data.

Vegetation Mask. As illustrated in Figure 3, we take the union of the ALS-derived mask indicating vegetation over 1.5m in height, with the official forest plots outlines, both provided by IGN [31, 60]. The resulting vegetation mask covers trees and shrubs within forest plots as well as outside, such as hedges and urban trees. In contrast, canopy height estimation methods often only report evaluation of their prediction within forest outlines [9].

3.2 Evaluated Models

We evaluate different state-of-the-art computer vision approaches for canopy height estimation from a single VHR satellite image with 4 spectral bands. We list below the selected models and how we adapted them to our task.

Selected Models. Given the ubiquity of convolutional models for canopy height estimation, we evaluate the **UNet** [33] and **DeepLabv3** [61] architectures. We select Vision Transformers (**ViT**) and their convolutional-hybrid variant (**HViT**) [34], as they recently became standard in computer vision. We also explore hierarchical ViT architectures such as **SWIN** [40], **PCPVT** [41], and **PVTv2** [12].

To assess the impact of pretraining, we include models pretrained on **ImageNet** [62, 62], but also large external datasets such as **DinoV2** [39] and **CLIP-OPENAI** [63]. We also consider the **ScaleMAE** [64] model, pretrained on satellite imagery of various resolutions, and the model provided by Tolan et al. [7] for canopy height estimation from RGB images.

Input and Output Layer. As the models considered are originally designed for the semantic segmentation of RGB images, we adapt their architecture to our setting. To add the near-infrared channel, we change the input size from 3 to 4. We retain the pretrained weights related to RGB, and initialize the near-infrared channel weights with small random values drawn from a normal distribution $\mathcal{N}(0, 0.01)$. We replace the class prediction layer with a simple linear layer to predict continuous canopy heights and use the L_1 norm as a loss function.

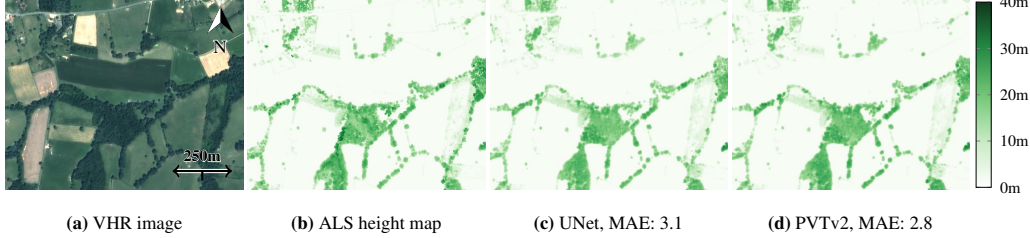


Figure 4: Qualitative Illustration. We select an area of interest and represent the available VHR image (a) and ground truth height map (b), as well as the predicted height map for UNet (c) and PVTv2 (d) models. We report the MAE within the vegetation mask.

Table 2: Canopy Height Prediction Models. We benchmark several backbone models for the task of predicting the canopy height of each pixel from a single satellite image. All models are pretrained on vision datasets and fine-tuned on our training set.

Model	pretraining	MAE in m	nMAE in %	RMSE in m	Bias in m	Tree cov. IoU in %
UNet ⁴ [33]	ImageNet1k [67]	2.67	23.8	4.18	-0.30	90.4
DeepLabv1 ¹ [61]	ImageNet1k [67]	3.18	28.4	4.83	-0.26	88.0
ViT-B ³ [34]	ImageNet21k [61]	4.26	37.8	6.06	-0.84	86.0
HViT ³ [34]	ImageNet21k [61]	2.65	24.0	4.18	-0.13	90.2
PCPVT ³ [41]	ImageNet1k [61]	2.57	23.1	4.06	-0.17	90.4
SWIN ³ [40]	ImageNet21k [61]	2.54	22.8	4.00	-0.11	90.5
PVTv2 ³ [12]	ImageNet1k [61]	2.52	22.9	4.02	0.00	90.5
ScaleMAE ⁵ [64]	FotM [68]	3.45	31.2	5.13	-0.48	88.2
ViT-B ³ [34]	DINOv2[39]	4.84	43.2	6.68	-0.48	84.8
ViT-B ² [34]	CLIP_OPENAI [63]	2.87	25.9	4.43	-0.07	89.7
ViT-L ⁶ [34]	Tolan[7]	4.46	38.9	6.27	-1.03	85.6

Dataloader and Evaluation. During training, we sample random tiles of size 224×224 . For inference, we sample tiles of the same size on the test sets along a regular grid with 50% overlap, and only retain the center half of each prediction. We train our model to predict the canopy height for all pixels, which may include heights that do not correspond to trees. However, we only compute the evaluation metrics for pixels within the vegetation mask described in Section 3.1.

Parameters and Resources. We use a batch size of 64 with random scaling of 0.5 to 2 and random rotations (0, 90, 180, or 270°). We use the ADAM optimizer [65] with a learning rate of 10^{-3} , a linear warmup of 1 epoch, and a ReduceLROnPlateau scheduler [66] with a patience of 1 and a decay of 0.5. We perform early stopping with a patience of 3. These hyperparameters were selected by considering their impact on the UNet and ViT models. Reproducing our experiments requires 1260 GPU-h with A100 GPUs. We estimate our hyperparameters search and initial experiments to 1800 GPU-h. We use a combination of internal clusters and the HPC GENCI.

3.3 Results and Analysis

Setting. We evaluate the vision models presented in Table 2, as well as the accuracy of existing canopy maps that we interpolate to our ground truth resolution of 1.5m per pixel. This evaluation, however, is subject to limitations: (i) unknown training sets for some models might lead to data contamination; (ii) interpolation might distort results, especially for the map of Tolan *et al.* which we downsample from 1m to 1.5m; (iii) potential discrepancies between the timing of the image used to predict the maps and our ALS acquisitions, (iv) maps derived at lower resolution are trained to predict the maximum canopy height in larger pixels, which bias them to higher values. Such factors affect the reliability of comparisons with other maps, which are given as indicative. By releasing all related data and metadata openly, we aim to mitigate these issues for future evaluations.

Table 3: Canopy Height Maps Evaluation. We evaluate on our test set several of the available canopy height map products obtained by previous works.

Map	Backbone	res. in m	MAE in m	nMAE in %	RMSE in m	Bias in m	Tree cov. IoU in %
Potapov [11]	UNet	30	6.27	58.1	8.68	1.79	78.0
Schwartz [9, 70]	UNet	10	5.17	42.7	7.20	3.37	76.8
Lang [10]	CNN	10	9.22	89.5	17.14	8.40	77.4
Liu [8]	UNet	3.0	4.83	46.6	6.90	1.56	84.1
Tolan [7]	ViT-L	1.0	5.07	43.7	7.15	-2.95	78.8
Open-Canopy	UNet	1.5	2.67	23.8	4.18	-0.30	90.4
Open-Canopy	PVTv2	1.5	2.52	22.9	4.02	0.00	90.5

Metrics. We evaluate the performance of canopy height estimation models with five metrics: Root Mean Square Error (**RMSE**), Mean Absolute Error (**MAE**), normalized MAE (**nMAE**)—which normalizes the absolute error by the actual height, **Bias**—the error averaged across the test set, and Intersection over Union (IoU) for **Tree Cover** predictions. The tree cover IoU is calculated by comparing binary maps generated by thresholding both ground truth and predicted height maps at a 2m threshold. All metrics are computed only on pixels within the vegetation mask and with ground truth height below 60m. The nMAE is calculated only for pixels with ground truth heights above 2m.

Analysis. We report the quantitative performance of all evaluated backbones in Table 2, and selected illustrations in Figure 4. We make the following observations:

- **Impact of Backbones.** Contrary to trends in natural image analysis, convolution-based approaches (UNet, HVIT) outperform ViTs, indicating that convolutions can efficiently extract relevant local features. However, hierarchical ViTs (SWIN, PCPVT, PVTv2) achieve the highest precision, underscoring the multi-scale structure of the task.
- **Impact of Pretraining.** Interestingly, models pre-trained on ImageNet (UNet, PVTv2) perform better than foundation models trained on extensive databases of natural images (CLIP, DINO). These models do not generalize well to canopy height estimation, likely due to differences in viewpoint, task specificity, data type, and available spectral bands. ScaleMAE and Tolan’s ViT, despite being trained on satellite images, do not adapt well to our task. We hypothesize that this is due to the spatial domain shift and the fact that they are trained without the infrared channel.
- **Overall Performance.** The methods assessed in this benchmark exhibit commendable results, achieving tree cover detection with over 90% IoU and an nMAE around 20% for the best-performing models.

Comparison with Existing Maps. In Table 3, we evaluate the precision of canopy height maps generated by UNet and PVTv2 networks trained on the Open-Canopy dataset against those from other research. With the caveats on the fairness of the comparison mentioned above, our maps achieve significantly better precision. The low performance of models derived from low-resolution imagery is expected, as they are trained to estimate tree height at a different resolution. Among the ALS-based methods, Liu *et al.*’s model performs best, likely due to its training data from Europe, which differs from Tolan et al.’s training in the continental US. Moreover, the Tolan *et al.* model relies solely on RGB data, while the inclusion of near-infrared is proven to be highly discriminative for vegetation analysis [69]. In Figure 5, we report error plots across various vegetation height bins, highlighting that the PVTv2 model trained on Open-Canopy exhibits significantly lower bias and superior performance, especially in areas with tall trees.

3.4 Limitations

Our dataset, while robust, has several limitations:

- **Geographic Focus:** Although metropolitan France offers a unique combination of open-access data and diverse landscapes, the geographic focus of Open-Canopy limits its global

¹ pytorch.org/vision ² huggingface.co/laion ³ timm.fast.ai/ ⁴ github.com/qubvel/segmentation_models.pytorch
⁵ github.com/bair-climate-initiative/scale-mae ⁶ github.com/facebookresearch/HighResCanopyHeight

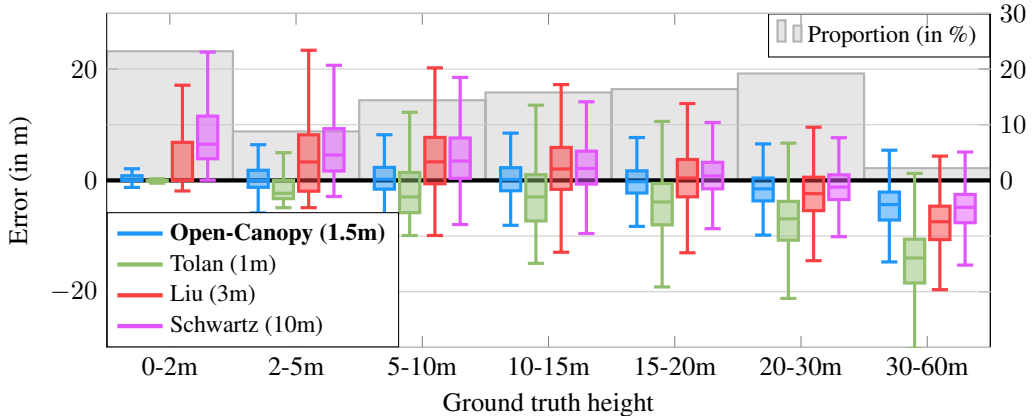


Figure 5: Distribution of Error. We plot the distribution of errors according to the ground truth canopy height for a PVTv2 model trained on Open-Canopy and different canopy height map products.

benchmark for VHR canopy height prediction. In particular, it lacks critical forest types such as rainforests. We hope that France’s open-access policy and this benchmark will inspire other countries and leads to the creation of a truly global VHR canopy height dataset.

- **Limits of ALS:** The ALS-based canopy heights are derived from physical measurements using aerial LiDAR, which can introduce errors, such as those from multiple echoes. These errors are mitigated by LiDAR-HD’s outlier removal, but cannot be excluded without costly in-situ drone-based measurements. Moreover, while SPOT 6-7 images are from spring and summer, LiDAR measurements are from all seasons.
- **Biomass Estimation:** Canopy height alone is an imperfect proxy for biomass as it does not take into account the multi-layered structure and density of tree.

4 Open-Canopy- Δ : Detecting Canopy Height Changes

In this section, we present Open-Canopy- Δ , our auxiliary benchmark for the task of canopy height change detection. We first present the dataset (Section 4.1), then our results Section 4.2

4.1 Dataset Characteristics

We introduce Open-Canopy- Δ , a new benchmark for detecting vegetation change between consecutive VHR images. We define changes as areas in which the canopy height has significantly decreased.

Extent and Context. We study the Forêt de Chantilly, a declining forest due to climate change and of high concern for conservationists [71]. We consider two ALS acquisitions in February 2022 [31] and September 2023 [71], allowing us to build their respective height maps and collect their associated SPOT 6-7 images. In total, the spatial extent of the area of interest is 166,340 hectares. Note that this area does *not* overlap with the training set of Open-Canopy.

Processing. We first construct a rasterized canopy change map by subtracting the first ALS-based height map from the later one. Change in canopy height can be due to forest disturbance events, such as fires, clear or partial cuts, or maintenance pruning. However, other unwanted elements can affect this measurement, such as seasonal growth cycles, wind, or sensor errors. To generate robust binary *change mask*, we focus on areas with significant, localized, and consistent decreases in canopy height. In practice, the canopy change masks are obtained as follows: (i) we select pixels showing a loss exceeding 10m, (ii) we regularize the resulting binary masks with morphological operations: erosion with a kernel of 3-pixel edge, two iterations dilation with a 3-pixel edge kernel, and finally erosion with a 3-pixel edge kernel, and (iii) we remove connected components smaller than 100m². See Figure 6 for illustrations and the supplementary for more details on the choice of hyperparameters.

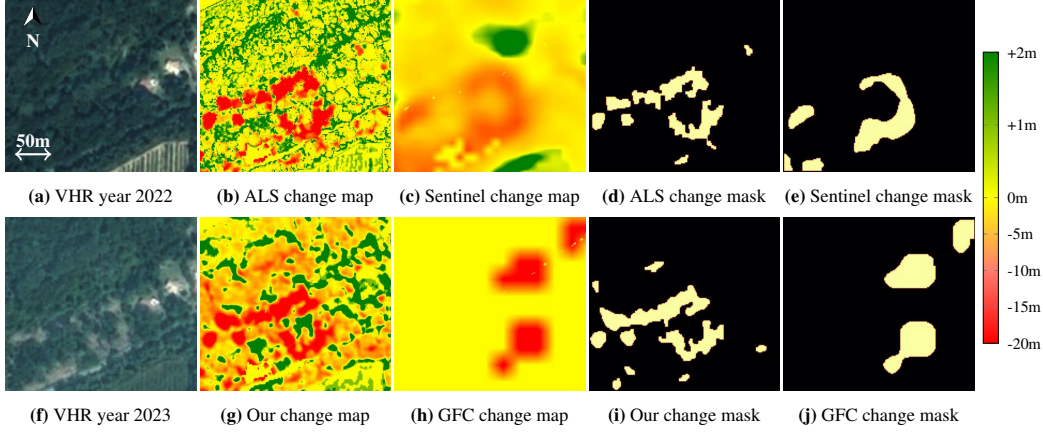


Figure 6: Canopy Height Change. We consider VHR images taken in 2022 and 2023 in Chantilly Forest (a and f), and use ALS observations of the same years to derive a canopy height change map (b). We compare this map to the ones predicted by a PVTv2 model (g) and two competing approaches: Sentinel-derived maps from Schwartz [9] (c) and Global Forest Change [42] (h). Finally, we compare the binary change masks derived from ALS measurements (d) and from predicted change maps (e,i,j).

Table 4: Forest Change Mask Evaluation. We evaluate our best model (PVTv2) for the task of detecting canopy height change masks. We also evaluate canopy height maps from

	Precision (%)	Recall (%)	F1 score (%)	IoU (%)
Schwartz [9]	32.7	4.6	8.0	4.2
Global Forest Change [42]	0.6	5.4	1.0	0.5
Open-Canopy (ours)	29.5	48.8	36.8	22.5

4.2 Results and Analysis

We evaluate different approaches for the task of estimating the difference in canopy height between two VHR images, which holds significant applications in forestry management.

Setting. As shown in Figure 6, we provide models with two VHR satellite images corresponding to two consecutive years. We generate a canopy change map by subtracting the canopy height maps predicted by our model from these two images. We do not directly compare the change maps, as the precision of canopy height estimation can be larger than normal tree growth. Instead, we apply the preprocessing described in Section 4.1 to produce predicted binary canopy height change masks.

Metrics. We evaluate the predicted canopy height change masks by computing the pixel-wise **Precision**, **Recall**, **F1 score**, and **IoU** with respect to the ALS-derived masks. **Results.** We compare height change masks predicted by a PVTv2 model trained on Open-Canopy with those derived from height maps provided by [9] and Global Forest Change [42]. As detailed in Table 4, our model achieves significantly better performance than other methods, although precision remains a challenge. Figure 6 illustrates that while our predicted change maps do not perfectly align with the ground truth maps—which also suffer from minor registration errors—the consistency of our predictions suggests their potential utility in detecting significant year-to-year changes.

5 Conclusion

We introduced Open-Canopy, the first country-scale, open-access benchmark combining VHR satellite imagery with ALS-derived canopy height measurements. We evaluated multiple recent state-of-the-art computer vision models for the task of canopy height estimation. Despite the dominance of convolutional networks in prior works, our findings suggest that transformer-based architectures exhibit superior performance. We also proposed Open-Canopy- Δ , a benchmark for detecting canopy height change detection from consecutive observations, a difficult task, even for the best-performing

models. We hope that our dataset and benchmarks will encourage the computer vision community to further explore canopy height estimation as a standard task for evaluating new architectures and inspire forestry experts to design bespoke architectures.

6 Acknowledgment

The experiments conducted in this study were performed using HPC/AI resources provided by GENCI-IDRIS (Grant 2023-AD010114718 and 2023-AD011014781) and Inria.

References

- [1] Erkki Tomppo, Thomas Gschwantner, Mark Lawrence, Ronald E McRoberts, Karl Gabler, K Schadauer, Claude Vidal, A Lanz, Göran Ståhl, Emil Cienciala, et al. National forest inventories. *Pathways for Common Reporting. European Science Foundation*, 2010.
- [2] French Ministry of Agriculture. The national forest and wood programme (PNFB). <https://agriculture.gouv.fr/telecharger/84443?token=a8749378b10811200dbd491dae3a854f4b56903f584821e2e9d0f6f3862e8577>, 2024. [Online; accessed 12-May-2024].
- [3] Fabian Ewald Fassnacht, Christoph Mager, Lars T Waser, Urša Kanjir, Jannika Schäfer, Ana Potocnik Buhvald, Elham Shafeian, Felix Schiefer, Liza Stančić, Markus Immittizer, et al. Forest practitioners' requirements for remote sensing-based canopy height, wood-volume, tree species, and disturbance products. *Forestry: An International Journal of Forest Research*, 2024.
- [4] Rodney J Keenan. Climate change impacts and adaptation in forest management: A review. *Annals of forest science*, 2015.
- [5] Ronald E McRoberts and Erkki O Tomppo. Remote sensing support for national forest inventories. *Remote sensing of environment*, 2007.
- [6] David LA Gaveau and Ross A Hill. Quantifying canopy height underestimation by laser pulse penetration in small-footprint airborne laser scanning data. *Canadian Journal of Remote Sensing*, 2003.
- [7] Jamie Tolan, Hung-I Yang, Benjamin Nosarzewski, Guillaume Couairon, Huy V Vo, John Brandt, Justine Spore, Sayantan Majumdar, Daniel Haziza, Janaki Vamaraju, et al. Very high resolution canopy height maps from RGB imagery using self-supervised vision transformer and convolutional decoder trained on aerial LiDAR. *Remote Sensing of Environment*, 2024.
- [8] Siyu Liu, Martin Brandt, Thomas Nord-Larsen, Jerome Chave, Florian Reiner, Nico Lang, Xiaoye Tong, Philippe Ciais, Christian Igel, Adrian Pascual, et al. The overlooked contribution of trees outside forests to tree cover and woody biomass across Europe. *Science Advances*, 2023.
- [9] Martin Schwartz, Philippe Ciais, Aurélien De Truchis, Jérôme Chave, Catherine Ottlé, Cedric Vega, Jean-Pierre Wigneron, Manuel Nicolas, Sami Jouaber, Siyu Liu, Martin Brandt, and Ibrahim Fayad. FORMS: Forest multiple source height, wood volume, and biomass maps in France at 10 to 30m resolution based on Sentinel-1, Sentinel-2, and GEDI data with a deep learning approach. *Earth System Science Data*, 2023.
- [10] Nico Lang, Walter Jetz, Konrad Schindler, and Jan Dirk Wegner. A high-resolution canopy height model of the Earth. *Nature Ecology & Evolution*, 2023.
- [11] Peter Potapov, Xinyuan Li, Andres Hernandez-Serna, Alexandra Tyukavina, Matthew C Hansen, Anil Kommarreddy, Amy Pickens, Svetlana Turubanova, Hao Tang, Carlos Edibaldo Silva, et al. Mapping global forest canopy height through integration of GEDI and Landsat data. *Remote Sensing of Environment*, 2021.
- [12] Wenhui Wang, Enze Xie, Xiang Li, Deng-Ping Fan, Kaitao Song, Ding Liang, Tong Lu, Ping Luo, and Ling Shao. PVTv2: Improved baselines with pyramid vision transformer.

Computational Visual Media, 2022.

- [13] Ekaterina Kalinicheva, Loic Landrieu, Clément Mallet, and Nesrine Chehata. Multi-layer modeling of dense vegetation from aerial LiDAR scans. In *CVPR Workshop Earth Vision*, 2022.
- [14] Stéphane Lecq, Anne Loisel, Francois Brischoux, Stephen J Mullin, and Xavier Bonnet. Importance of ground refuges for the biodiversity in agricultural hedgerows. *Ecological Indicators*, 2017.
- [15] Stephan Getzin, Kerstin Wiegand, and Ingo Schöning. Assessing biodiversity in forests using very high-resolution images and unmanned aerial vehicles. *Methods in ecology and evolution*, 2012.
- [16] Nathan L Stephenson, AJ Das, R Condit, SE Russo, PJ Baker, Noelle G Beckman, DA Coomes, ER Lines, WK Morris, Nadja Rüger, et al. Rate of tree carbon accumulation increases continuously with tree size. *Nature*, 2014.
- [17] Hans Pretzsch, Miren Del Río, Catia Arcangeli, Kamil Bielak, Małgorzata Dudzinska, David Ian Forrester, Joachim Klädtke, Ulrich Kohnle, Thomas Ledermann, Robert Matthews, et al. Forest growth in Europe shows diverging large regional trends. *Scientific Reports*, 2023.
- [18] Adrian J Das and Nathan L Stephenson. Improving estimates of tree mortality probability using potential growth rate. *Canadian Journal of Forest Research*, 2015.
- [19] Claudia Huertas, Daniel Sabatier, Géraldine Derroire, Bruno Ferry, Toby D Jackson, Raphaël Pélissier, and Grégoire Vincent. Mapping tree mortality rate in a tropical moist forest using multi-temporal LiDAR. *International Journal of Applied Earth Observation and Geoinformation*, 2022.
- [20] Xiaowei Yu, Juha Hyyppä, Harri Kaartinen, and Matti Maltamo. Automatic detection of harvested trees and determination of forest growth using airborne laser scanning. *Remote sensing of Environment*, 2004.
- [21] Tobias Kuemmerle, Oleh Chaskovskyy, Jan Knorn, Volker C Radeloff, Ivan Kruhlov, William S Keeton, and Patrick Hostert. Forest cover change and illegal logging in the Ukrainian Carpathians in the transition period from 1988 to 2007. *Remote Sensing of Environment*, 2009.
- [22] Sara T Thompson and William B Magrath. Preventing illegal logging. *Forest Policy and Economics*, 2021.
- [23] Gabriel Popkin. The hunt for the world's missing carbon. *Nature*, 2015.
- [24] Ruth D Yanai, Craig Wayson, Donna Lee, AB Espejo, John Law Campbell, Mark B Green, Jenna M Zukswert, SB Yoffe, JE Aukema, AJ Lister, et al. Improving uncertainty in forest carbon accounting for REDD+ mitigation efforts. *Environmental research letters*, 2020.
- [25] Roger A Sedjo. The carbon cycle and global forest ecosystem. *Water, Air, and Soil Pollution*, 1993.
- [26] Gregory P Asner, Michael Keller, Rodrigo Pereira, Jr, Johan C Zweede, and Jose NM Silva. Canopy damage and recovery after selective logging in Amazonia: Field and satellite studies. *Ecological Applications*, 2004.
- [27] Colbert M Jackson and Elhadi Adam. Remote sensing of selective logging in tropical forests: Current state and future directions. *iForest-Biogeosciences and Forestry*, 2020.
- [28] Ralph Dubayah, James Bryan Blair, Scott Goetz, Lola Fatoyinbo, Matthew Hansen, Sean Healey, Michelle Hofton, George Hurt, James Kellner, Scott Luthcke, et al. The global ecosystem dynamics investigation: High-resolution laser ranging of the Earth's forests and topography. *Science of remote sensing*, 2020.
- [29] Ralph Dubayah, John Armston, Sean P Healey, Jamis M Bruening, Paul L Patterson, James R Kellner, Laura Duncanson, Svetlana Saarela, Göran Ståhl, Zhiqiang Yang, et al. GEDI launches a new era of biomass inference from space. *Environmental Research Letters*, 2022.

[30] FH Wagner, S Roberts, AL Ritz, G Carter, R Dalagnol, S Favrichon, M Hirye, M Brandt, P Ciais, and S Saatchi. Sub-meter tree height mapping of California using aerial images and LiDAR-informed U-Net model. *Remote Sensing of Environment*, 2024.

[31] IGN. LiDAR HD : Vers une nouvelle cartographie 3d du territoire. <https://www.ign.fr/institut/lidar-hd-vers-une-nouvelle-cartographie-3d-du-territoire>, 2024. [Online; accessed 12-May-2024].

[32] DINAMIS. French national facility for institutional procurement of vhr satellite imagery. <https://openspot-dinamis.data-terra.org>, 2024. [Online; accessed 12-May-2024].

[33] Olaf Ronneberger, Philipp Fischer, and Thomas Brox. UNet: Convolutional networks for biomedical image segmentation. In *MICCAI*. Springer, 2015.

[34] Alexey Dosovitskiy, Lucas Beyer, Alexander Kolesnikov, Dirk Weissenborn, Xiaohua Zhai, Thomas Unterthiner, Mostafa Dehghani, Matthias Minderer, Georg Heigold, Sylvain Gelly, et al. An image is worth 16x16 words: Transformers for image recognition at scale. In *International Conference on Learning Representations*, 2020.

[35] Xin Bao, Rui Zhang, Jichao Lv, Renzhe Wu, Hongsheng Zhang, Jie Chen, Bo Zhang, Xiaoying Ouyang, and Guoxiang Liu. Vegetation descriptors from Sentinel-1 SAR data for crop growth monitoring. *ISPRS Journal of Photogrammetry and Remote Sensing*, 2023.

[36] Matthias Drusch, Umberto Del Bello, Stefane Carlier, Olivier Colin, Valérie Fernandez, Ferran Gascon, Bianca Hoersch, Claudia Isola, Paolo Laberinti, Philippe Martimort, Aimé Meygret, François Spoto, Omar Sy, Franco Marchese, and Pier Bargellini. Sentinel-2: ESA's optical high-resolution mission for GMES operational services. *Remote Sensing of Environment*, 2012.

[37] United States Department of Agriculture. National agriculture imagery program (NAIP). https://www.fsa.usda.gov/Assets/USDA-FSA-Public/usdafiles/APFO/support-documents/pdfs/naip_infosheet_2016.pdf, 2024. [Online; accessed 12-May-2024].

[38] Anouk Schleich, Sylvie Durrieu, and Cédric Vega. Improving gedi footprint geolocation using a high resolution digital elevation model. *IEEE Journal of Selected Topics in Applied Earth Observations and Remote Sensing*, 2023.

[39] Maxime Oquab, Timothée Darzet, Théo Moutakanni, Huy V Vo, Marc Szafraniec, Vasil Khalidov, Pierre Fernandez, Daniel HAZIZA, Francisco Massa, Alaaeldin El-Nouby, et al. DINOv2: Learning robust visual features without supervision. *TMLR*, 2023.

[40] Ze Liu, Yutong Lin, Yue Cao, Han Hu, Yixuan Wei, Zheng Zhang, Stephen Lin, and Baining Guo. SWIN transformer: Hierarchical vision transformer using shifted windows. In *ICCV*, 2021.

[41] Xiangxiang Chu, Zhi Tian, Yuqing Wang, Bo Zhang, Haibing Ren, Xiaolin Wei, Huaxia Xia, and Chunhua Shen. Twins: Revisiting the design of spatial attention in vision transformers. *NeurIPS*, 2021.

[42] Matthew C Hansen, Peter V Potapov, Rebecca Moore, Matt Hancher, Svetlana A Turubanova, Alexandra Tyukavina, David Thau, Stephen V Stehman, Scott J Goetz, Thomas R Loveland, and others. High-resolution global maps of 21st-century forest cover change. 2013.

[43] Kenneth G MacDicken. Global forest resources assessment 2015: What, why and how? *Forest Ecology and Management*, 2015.

[44] Kenneth G MacDicken, Phosiso Sola, John E Hall, Cesar Sabogal, Martin Tadoum, and Carlos de Wasseige. Global progress toward sustainable forest management. *Forest Ecology and Management*, 2015.

[45] Jushuang Qin, Menglu Ma, Yutong Zhu, Baoguo Wu, and Xiaohui Su. 3PG-MT-LSTM: A hybrid model under biomass compatibility constraints for the prediction of long-term forest growth to support sustainable management. *Forests*, 2023.

[46] Long Ye, Lei Gao, Raymundo Marcos-Martinez, Dirk Mallants, and Brett A Bryan. Projecting Australia's forest cover dynamics and exploring influential factors using deep learning. *Environmental Modelling & Software*, 2019.

[47] Guan Peng and ZHENG Yili. Research on forest phenology prediction based on LSTM and GRU model. *Journal of Resources and Ecology*, 2022.

[48] Christopher PO Reyer, Ramiro Silveyra Gonzalez, Klara Dolos, Florian Hartig, Ylva Hauf, Matthias Noack, Petra Lasch-Born, Thomas Rötzer, Hans Pretzsch, Henning Meesenburg, et al. The PROFOUND database for evaluating vegetation models and simulating climate impacts on European forests. *Earth System Science Data*, 2020.

[49] Yousef Erfanifard, Mohsen Lotfi Nasirabad, and Krzysztof Stereńczak. Assessment of Iran's mangrove forest dynamics (1990–2020) using Landsat time series. *Remote Sensing*, 2022.

[50] Mathieu Decuyper, Roberto O Chávez, Madelon Lohbeck, José A Lastra, Nandika Tsendbazar, Julia Hackländer, Martin Herold, and Tor-G Vågen. Continuous monitoring of forest change dynamics with satellite time series. *Remote Sensing of Environment*, 2022.

[51] Shohei Kameyama and Katsuaki Sugiura. Estimating tree height and volume using unmanned aerial vehicle photography and SfM technology, with verification of result accuracy. *Drones*, 2020.

[52] Yanchao Zhang, Hanxuan Wu, and Wen Yang. Forests growth monitoring based on tree canopy 3D reconstruction using UAV aerial photogrammetry. *Forests*, 2019.

[53] Etalab. Open licence 2.0. <https://www.etalab.gouv.fr/wp-content/uploads/2018/11/open-licence.pdf>, 2024. [Online; accessed 12-May-2024].

[54] Murray C Peel, Brian L Finlayson, and Thomas A McMahon. Updated world map of the Köppen-Geiger climate classification. *Hydrology and earth system sciences*, 2007.

[55] IGN. More than 190 tree species inventoried in france. <https://inventaire-forestier.ign.fr/spip.php?article175>, 2024. [Online; accessed 12-May-2024].

[56] Fiches descriptives des grandes régions écologiques (GRECO) et des sylvoécorégions (SER). <https://inventaire-forestier.ign.fr/spip.php?article773>. Accessed: 2024-04-29.

[57] Gary S Smith. Digital orthophotography and GIS. In *Proceedings of the 1995 ESRI user conference*, 1995.

[58] Guo Dong Yang and Xiang Zhu. Ortho-rectification of SPOT 6 satellite images based on RPC models. *Applied Mechanics and Materials*, 2013.

[59] Alan R Gillespie, Anne B Kahle, and Richard E Walker. Color enhancement of highly correlated images. ii. channel ratio and “chromaticity” transformation techniques. *Remote Sensing of Environment*, 1987.

[60] IGN. Forest data base. <https://geoservices.ign.fr/bdforet>, 2024. [Online; accessed 12-May-2024].

[61] Liang-Chieh Chen, George Papandreou, Florian Schroff, and Hartwig Adam. Rethinking atrous convolution for semantic image segmentation. *arXiv preprint arXiv:1706.05587*, 2017.

[62] Tal Ridnik, Emanuel Ben-Baruch, Asaf Noy, and Lihi Zelnik-Manor. ImageNet-21K pretraining for the masses. In *NeurIPS Datasets and Benchmarks Track*, 2021.

[63] Alec Radford, Jong Wook Kim, Chris Hallacy, Aditya Ramesh, Gabriel Goh, Sandhini Agarwal, Girish Sastry, Amanda Askell, Pamela Mishkin, Jack Clark, et al. Learning transferable visual models from natural language supervision. In *ICML*, 2021.

[64] Colorado J Reed, Ritwik Gupta, Shufan Li, Sarah Brockman, Christopher Funk, Brian Clipp, Kurt Keutzer, Salvatore Candido, Matt Uyttendaele, and Trevor Darrell. Scale-MAE: A scale-

aware masked autoencoder for multiscale geospatial representation learning. In *ICCV*, 2023.

[65] Diederik P Kingma and Jimmy Ba. Adam: A method for stochastic optimization. *ICLR*, 2015.

[66] PyTorch: ReduceLROnPlateau. https://pytorch.org/docs/stable/generated/torch.optim.lr_scheduler.ReduceLROnPlateau.html#torch.optim.lr_scheduler.ReduceLROnPlateau. Accessed: 2024-02-29.

[67] Olga Russakovsky, Jia Deng, Hao Su, Jonathan Krause, Sanjeev Satheesh, Sean Ma, Zhiheng Huang, Andrej Karpathy, Aditya Khosla, Michael Bernstein, et al. ImageNet large scale visual recognition challenge. *IJCV*, 2015.

[68] Gordon Christie, Neil Fendley, James Wilson, and Ryan Mukherjee. Functional map of the world. In *CVPR*, 2018.

[69] Toby N Carlson and David A Ripley. On the relation between NDVI, fractional vegetation cover, and leaf area index. *Remote sensing of Environment*, 1997.

[70] Martin Schwartz. *Mapping forest height and biomass at high resolution in France with satellite remote sensing and deep learning*. PhD thesis, Université Paris-Saclay, 2023.

[71] Institut de France. Collectif sauvons la foret de chantilly. <https://chateaudechantilly.fr/la-foret/ensemble-sauvons-la-foret-de-chantilly/>, 2024. [Online; accessed 12-May-2024].

Appendix

A-1 Additional Evaluations

We present several supplementary experiments to evaluate the impact on the performance of the tree height (Section A-1.1), the spatial resolution of the evaluation (Section A-1.1), and the parameters of the canopy height change processing (Section A-1.3).

A-1.1 Influence of Tree Height

We provide in Table A-1 an evaluation of canopy height estimation for different ranges of height.

- Note that the nMAE (normalized Mean Absolute Error) is computed for all ranges as the average of the pixel-wise normalized absolute error:

$$\text{nMAE} = \frac{|(z_{\text{true}} - z_{\text{pred}})|}{1 + z_{\text{true}}}, \quad (\text{A-1})$$

where z_{true} and z_{pred} are respectively the ALS-derived and predicted height for a given pixel. The additional term in the denominator makes this measure more robust for pixels corresponding to low vegetation.

- When computing the nMAE for the 0-60 m range, we actually exclude the 0-2m bin. Indeed, even with the regularization, these values tend to be very large and dominate the metric. Furthermore, it makes the comparison unfair for maps with lower spatial resolution which aim to predict the highest pixel in a larger pixel, and may overlap with bare soil pixel at a higher resolution.

As shown in Table A-1 by the bias of our model for different ranges, our model tends to over-predict the height of small trees and under-predict the height of tall trees. While the average error is higher for larger trees, our model has the lowest nMAE for the 20-30m range, with a value of 12.1%.

A-1.2 Evaluation at a resolution of 10m

In order to provide a more fair evaluation for the models predicting canopy height at a 10 m resolution, we convert both our ground truth and predicted height map to a resolution of 10m and re-evaluate all available maps. We down-sample the height maps by taking for each 10m resolution pixel the maximum value of all 1.5m pixels it overlaps. This is equivalent to rasterizing the full ALS 3D point cloud to a 10m grid directly. We take the maximum value to be comparable to models that are trained on GEDI RH100 or RH95 (relative height at the 100th or 95th percentile).

We report the results in Table A-2, and observe a similar ordering than in Table 6 of the main paper. All methods see improved metrics as the problem is simpler, except for Tolan. In particular, the tree coverage problem becomes significantly easier at this resolution, with all 10 m-resolution methods nearing 90% IoU.

Note that the height map of [8] at a resolution of 3m was provided by the authors and is not available online.

A-1.3 Parameters of the Change Detection

We provide in Table A-3 an evaluation of canopy height change detection for different configurations of the ground truth binary change map. In particular, we consider the impact of the minimum height difference to be considered as a changed pixel, and the minimum contiguous change area below which we discard the components. Naturally, when only keeping large change areas, the problem becomes easier. The influence of the minimal tree height change is more ambiguous, as for large values, it implies precisely detecting the height of heigher trees, which is more difficult. Overall, while our choice of parameters (10 m and 100 m²) is arbitrary, it corresponds to changes that can be visually detected between two images, see Figure A-2.

Table A-1: Canopy Height Prediction Per Height Bins. We report the metrics for different bins of true tree height for the PVTv2[12] model.

Range in m	0-2	2-5	5-10	10-15	15-20	20-30	30-60	0-60
MAE in m	1.67	2.29	2.65	2.70	2.61	3.00	5.52	2.52
nMAE in %	138.8	53.6	32.1	20.3	14.3	12.1	16.0	22.9
RMSE in m	4.31	3.67	3.69	3.60	3.53	4.19	7.56	4.02
Bias in m	1.49	0.87	0.65	0.21	-0.42	-1.90	-5.31	0.00
Tree cov. IoU (%)	-	72.6	96.5	99.3	99.7	99.8	99.6	90.5

Table A-2: Canopy Height Prediction at 10m resolution. We resample all ground truth and predicted maps at on a 10 m grid.

Map	Backbone	Initial res. in m	MAE in m	nMAE in %	RMSE in m	Bias in m	Tree cov. IoU in %
Potapov [11]	UNet	30	6.17	44.6	8.33	-3.31	80.2
Schwartz [9, 70]	UNet	10	4.00	26.9	5.28	-1.38	90.1
Lang [10]	CNN	10	8.64	92.9	29.25	6.27	90.1
Liu [8]	UNet	3.0	4.58	37.4	10.97	-1.26	88.2
Tolan [7]	ViT-L	1.0	6.10	42.1	7.95	-5.37	81.6
Open-Canopy	UNet	1.5	2.72	19.0	3.95	-2.06	93.4
Open-Canopy	PVTv2	1.5	2.42	17.6	3.57	-1.69	93.3

A-2 Additional Illustrations

We provide here additional illustrations for qualitative assessment.

A-2.1 Canopy Height

See Figure A-1 for a comparison between the ALS-derived height map and the height map predicted from SPOT images. Our model is able to accurately predict the vegetation height in a variety of scenarios such as mountainous areas (first row), and detect small hedges on agricultural lands (second row). Our model can also handle dense forests (row 3 and 4) and urban environments (row 5), as well as mixed scenes (row 6 and 7). The high resolution of our predictions also allows for the identification of man-made features like forest paths, crucial for forest management.

A-2.2 Canopy Height Change

See Figure A-2 for more illustrations of height change detection. While our model tends to over predict small growth or loss of canopy height, the areas of strong disturbances—as denoted by our smoothed and filtered binary change maps—are overall well detected and delineated. Our illustration

Table A-3: Canopy Height Change Detection We compute the IoU metric (in %) for various minimum height difference (row, in m) and minimum contiguous area of change (column, in m^2). The values chosen in the benchmark are underlined.

	min surf	10 m^2	25 m^2	<u>100 m^2</u>	200 m^2	300 m^2	400 m^2
min diff							
-5 m		7.0	7.1	<u>7.2</u>	6.2	5.3	4.3
<u>-10 m</u>		17.1	17.9	22.5	23.5	25.0	28.6
-15 m		21.9	23.1	27.9	34.3	38.7	41.3
-20 m		18.4	19.7	29.5	35.7	30.0	31.5

covers areas of dense forests (first row) and mixed scenes (row 2 and 3). Our method can detect disturbances such as clear and selective cuts.

Note that the Sentinel-derived height maps for 2022 and 2023 were provided by the authors of [9], as only the map for 2020 is available online.

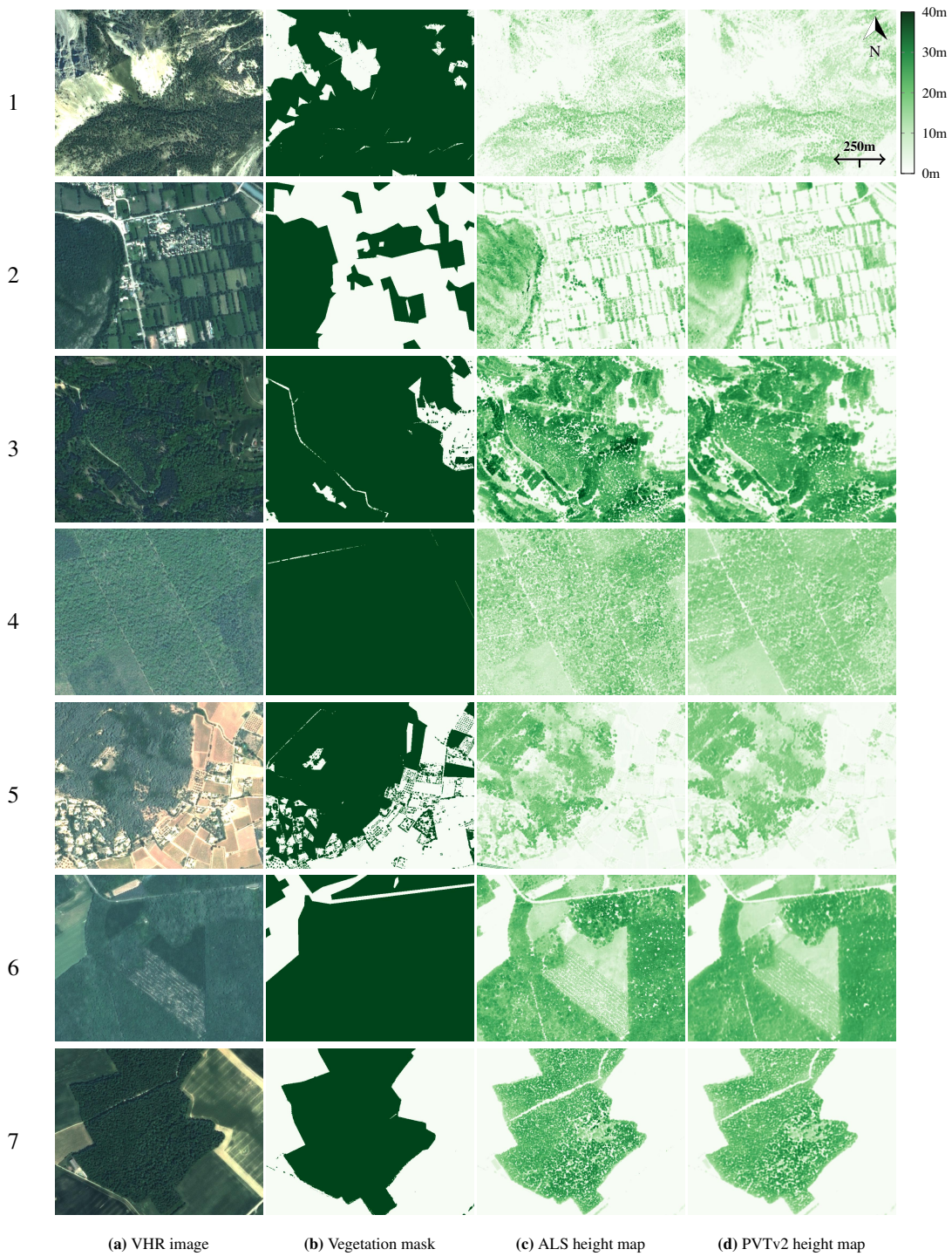


Figure A-1: Canopy Height Estimation Illustrations. We select seven areas of interest and represent the available VHR image (a), the vegetation mask used for evaluation (b), the ground truth ALS-derived height map (c), and the height map estimated with PVTv2 model from the VHR image (d). Scale and orientation are shared across all subfigures.

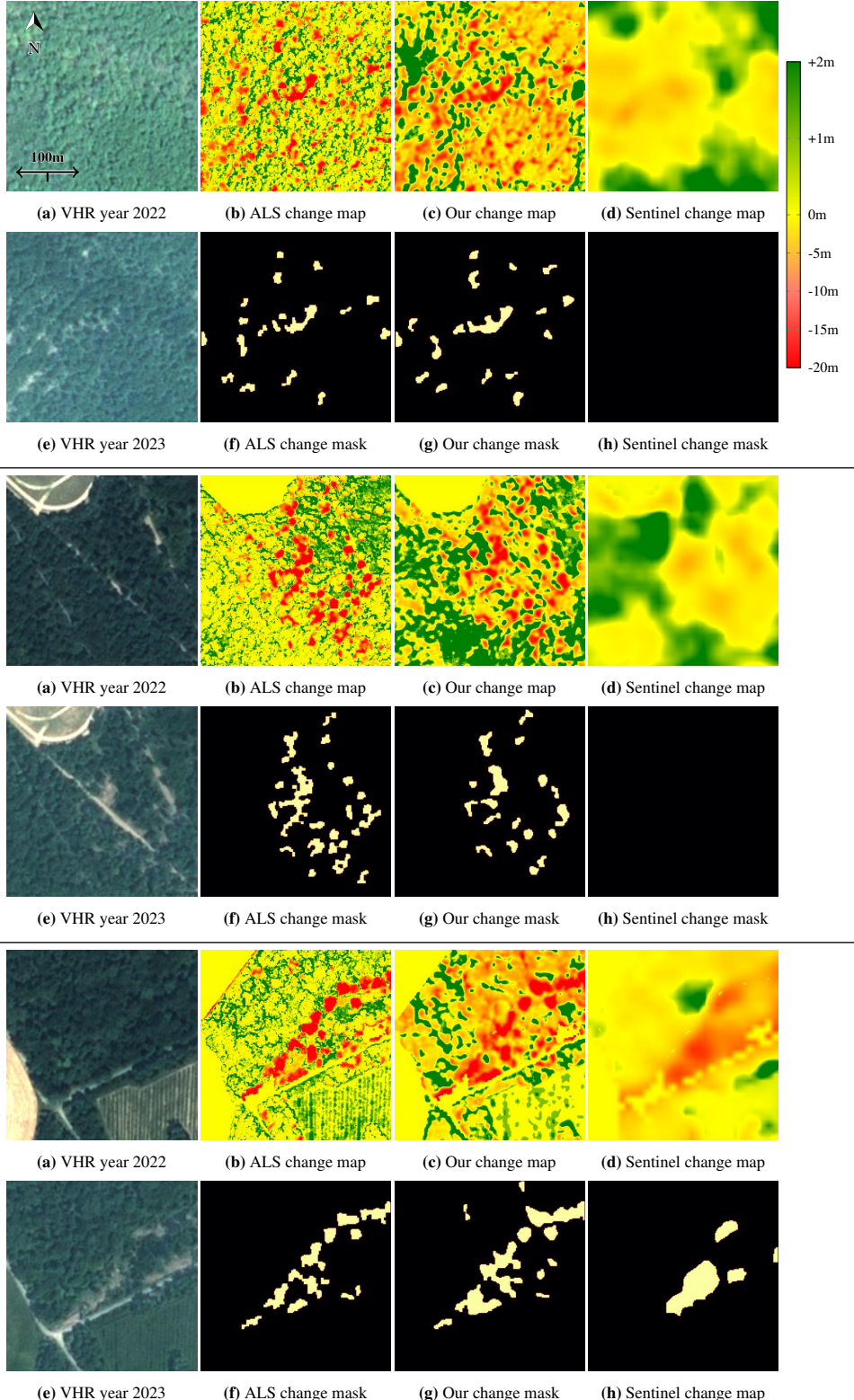


Figure A-2: Canopy Height Change. We consider VHR images taken in 2022 and 2023 in Chantilly Forest (a and e), and use ALS observations of the same years to derive a canopy height change map (b). We compare this map to the ones predicted by a PVTv2 model (c) and by a model from Schwartz trained on Sentinel data [9]. We also compare the binary change masks derived from ALS measurements (f) and from predicted change maps (g) and (h). Scale and orientation are shared across all subfigures.

A-3 Dataset description

A-3.1 Access

- The dataset is hosted on Huggingface platform (<https://huggingface.co/datasets/fajwel/Open-Canopy>), with download and usage instructions on the Open-Canopy project page hosted on GitHub (<https://github.com/fajwel/Open-Canopy>).
- The data is governed by the Open License 2.0 of Etalab (<https://www.etalab.gouv.fr/wp-content/uploads/2018/11/open-licence.pdf>).
- Codes for data preprocessing, training a custom model and evaluation are available at <https://github.com/fajwel/Open-Canopy>. The code for training all models of the benchmark will be released in the coming months along with their pretrained weights.

A-3.2 Composition

We describe here the organization of the dataset. See Section A-4 for details on how the dataset was prepared.

The dataset is organized in the following way:

- The folder `canopy_height` contains data for canopy height estimation.
- The folder `canopy_height_change` contains data for canopy height change estimation.

The composition of the `canopy_height` folder is the following:

- The file `geometries.geojson` stores a list of 95,429 $1km^2$ square geolocated geometries, giving access to the splits of the dataset. It can be loaded using the python package geopandas¹. Each geometry designates either a train, validation, test or buffer area. This information is stored in the column `split`. There are 8,046 buffer tiles, 66,339 train tiles, 7,369 validation tiles and 13,675 test tiles. Additionally, each geometry is associated to a year (corresponding to the year of the corresponding LiDAR acquisition), stored in the column `lidar_year`.
- The file `forest_mask.parquet` stores geolocated geometries of forests' outlines. It can be loaded using the python package geopandas. The parquet format is used to accelerate loading time.
- Each folder 2021, 2022 and 2023 contains three files:
 - `lidar.vrt` is a geolocalized virtual file that gives access to SPOT 6-7 images stored in the subfolder `spot`. It can be accessed through Qgis software² or python rasterio library³ for instance. It has the same extent as the geometries of the associated year.
 - Similarly `lidar.vrt` gives access to ALS-derived (LiDAR) canopy height maps stored in the subfolder `lidar`.
 - Similarly `lidar_classification.vrt` gives access to classification rasters stored in the subfolder `lidar_classification`.

The composition of the `canopy_height_change` folder is the following:

- The file `spot_1.tif` is a geolocalized image extracted from SPOT 6-7 images in the year 2022 in the area of Chantilly, France.
- The file `spot_2.tif` is a geolocalized image extracted from SPOT 6-7 images in the year 2023 in the area of Chantilly (France).
- The file `lidar_1.tif` is a geolocalized ALS-derived height map in the year 2022 in the area of Chantilly (France), derived from LiDAR HD [31].
- The file `lidar_2_m.tif` is a geolocalized ALS-derived height map in the year 2023 in the area of Chantilly (France), provided by [71], at a resolution of 1m, with height in meters, and covering only forests.

¹ <https://geopandas.org/en/stable/>

² <https://www.qgis.org/en/site/>

³ <https://rasterio.readthedocs.io/en/stable/>

- The file `pred_1.tif` is a geolocalized height map predicted by a PVTv2 model in 2022 in the area of Chantilly (France).
- The file `pred_2.tif` is a geolocalized height map predicted by a PVTv2 model in 2023 in the area of Chantilly (France).
- The file `lidar_classification.tif` is an ALS-derived classification raster in 2022 in the area of Chantilly (France).
- Additionally, files that follow the following pattern `*_masked.tif` designate images masked on the extent of the available ALS data for 2023.

A-3.3 Characteristics

- We provide SPOT 6-7 images, ALS-derived height maps and classification rasters covering 95,429 km² (including a "buffer" area of 8046 km², a train area of 66,339 km², a validation area of 7,369 km² and a test area of 13,675 km²). Each image has a resolution of 1.5m, with one annotation per pixel, for a total of 42,455,312,381 annotations.
- Additionally, we provide SPOT 6-7 imagery, ALS-derived height maps and a classification raster on the Chantilly forest area for 2022 and 2023 (571 km²).
- The Open-Canopy dataset is derived from a larger dataset of SPOT 6-7 acquisitions across the full metropolitan French territory between 2013 and 2023 ⁴, and a larger dataset of ALS acquisitions from the IGN campaign that started in 2021 and aims at covering the full metropolitan French territory (LiDAR HD) ⁵. The Open-Canopy dataset focuses on domains that are representative of the diversity of French forests and where LiDAR HD is available at the time of writing, with the goal of limiting the dataset's size to approximately 300 GB, in order to facilitate its usage by the machine learning community.
- Each SPOT image is at a resolution of 1.5 m per pixel, and features 4 spectral channels: red, blue, green, and near-infrared.
- Each height map image is at a resolution of 1.5 m per pixel, and features 1 channel (height in decimeters except if notified in the filename in the following format: "<name>_<unit>.tif").
- Each classification image is at a resolution of 1.5 m per pixel, and features 1 channel (classification ⁶ for a description of classes). Forests' outlines are stored as geometries in a parquet file. A Python utility is provided to create a vegetation mask from the classification raster and the forests' outlines.

A-4 Dataset preparation

A-4.1 SPOT 6-7 satellite imagery

- The aerial images are sampled from the DINAMIS ⁷ collection. This collection consists of an annual mosaic of selected tiles taken by SPOT 6-7 satellites between March and October of each year between 2013 and 2023, covering the entire French metropolitan territory. All images are orthorectified by IGN and mapped onto a unified cartographic coordinate reference system (Lambert 93). Each tile consists of an image with four spectral bands: red, green, blue, and near-infrared at a resolution of 6m, and an image with one panchromatic band at a resolution of 1.5m that can be downloaded separately.
- A total of 52 pairs of spectral and panchromatic images were downloaded from the DINAMIS website, for each year from 2021 to 2023, to cover a very diverse range of forest types in areas where LiDAR HD was available at the time of the creation of the dataset.
- We applied pansharpening with the weighted Brovey algorithm [59] to upsample all four spectral bands to a resolution of 1.5m, resulting in one image with four bands for each tile.
- We cropped each image to the area covered by the ALS acquisitions of the same year.
- Pixels values were clipped to a maximum value of 2000 to avoid outliers (upper bound both quantitatively and qualitatively assessed through histograms and visualization).

⁴ <https://openspot-dinamis.data-terra.org>

⁵ <https://geoservices.ign.fr/lidarhd>

⁶ https://geoservices.ign.fr/sites/default/files/2023-10/DC_LiDAR_HD_1-0 PTS.pdf

⁷ <https://openspot-dinamis.data-terra.org>

- Resulting images were normalized to a 0-255 range and saved as uint8 in a block-tiled compressed tiff format (256 × 256).
- The pansharpening and normalization procedures were voluntarily kept relatively simple in order to facilitate reproducibility. They may not be optimal for visualization, *e.g.*, lacking harmonization, but we expect deep learning models to be robust to such variations in input data.

A-4.2 ALS data

- The ALS classified point clouds were downloaded from the [LiDAR HD](#) website (IGN). A reference to each download link is saved in the file `geometries.geojson` in the column `lidar_url`.
- For each geometry, canopy height images were derived from ALS data by taking the maximum difference between the height of each point and the one of its nearest point classified as ground within its pixel, interpolating values in areas without data.
- LiDAR point clouds were classified by IGN into the main types of land cover (water, ground, high vegetation over 1.5m, buildings...). We use this classification to produce classification rasters at a resolution of 1.5m, where each pixel takes the value of the most frequent class of the corresponding LiDAR points.
- We then create vegetation masks by taking the union of the ALS-derived mask indicating vegetation over 1.5m in height, with the official forest plots outlines (file `forest_mask.parquet`), both provided by IGN. The resulting vegetation masks cover trees and shrubs within forest plots as well as outside, such as hedges and urban trees.
- The official forests' outlines were extracted from “BD foret” ⁸ and "simplified" using `geopandas` python library to a precision of 10m, with the goal to limit their size.

A-4.3 Splits

Our sampling strategy is semi-automated and proceeds as follows:

- SPOT images were associated to LiDAR height maps of the same year and geolocation (each LiDAR height map corresponds to a 1km² geolocalized square tile, referred to as “geometry” in the following).
- Geometries on overlapping areas between spot full images were removed.
- Geometries that had more than 100 zeros on the first spot band (*e.g.*, on edges of a full spot image) were discarded to avoid tiles with missing data.
- Test geometries of 1km² were sampled (with a fixed seed) to form contiguous squares of 7km² and to cover 20,000 km².
- Test geometries that overlapped each other were dropped.
- Test geometries that covered different years in terms of LiDAR acquisitions were dropped.
- This process resulted in a total test area of 13,675 km².
- A buffer of 1km was applied around each test area of 7km².
- Validation and train geometries were randomly sampled (with a fixed seed) among the remaining geometries, with a proportion of 10% for validation and 90% for training.
- This process resulted in a training area of 66,339 km² and a validation area of 7,369 km².

⁸ <https://geoservices.ign.fr/bdforet#telechargementv2>